

PRESTACK MIGRATION VELOCITY ANALYSIS USING TIME-REMIGRATION TRAJECTORIES

T. A. Coimbra, H. B. Santos, J. Schleicher and A. Novais

email: tgo.coimbra@gmail.com, js@ime.unicamp.br

keywords: Remigration, time-migration, migration velocity analysis, seismic velocity interpretation and processing

ABSTRACT

We present a prestack time-migration tool for local improvement of the seismic migration-velocity model. The method is based on time-remigration trajectories. It determines kinematic parameters using local-slope information of seismic reflection events. These parameters, in turn, are used to locally correct the velocity model. The main advantage of this technique is that it allows to carry out a moveout correction not just at a fixed point in a zero-offset (post-stack) time-migrated gather, but varying through all offsets of a common image gather (CIG), and taking into account the reflection-point displacement in the midpoint direction. In other words, it provides for migration velocity analysis (MVA) by time-remigration trajectories in prestack data. Tests on synthetic and SMAART-Sigsbee2B data show that the proposed tool not only increased the velocity-model resolution, but also provides a plausible time-migrated image.

INTRODUCTION

Migration velocity analysis (MVA) is an important seismic processing step in prestack time-imaging. Basically, MVA exploits the redundancy of seismic data to improve an a-priori velocity model. As first observed by Sattlegger (1975), seismic data from different offsets need to migrate to the same positions when using the correct velocity model. Hence, these images must be horizontally aligned, regardless of structure. However, the use of too low or too high migration velocities leads to offset-dependent mispositioning, known as migration smiles or frowns (Al-Yahya, 1989; Zhu et al., 1998).

Over the years, substantial effort has been directed towards the development of new MVA methods. Because of its conceptual clarity and simplicity, residual-moveout (RMO) analysis has become one of the favorite tools for MVA (Liu and Bleistein, 1995). Many algorithms are based on the moveout formula for a horizontal reflector (Al-Yahya, 1989). However, in the case of strongly dipping reflectors, this correction does not take into account the lateral displacement of the reflector image that is caused by a change in migration velocity, thus requiring iterative procedures. Schleicher and Biloti (2007) tried to improve Al-Yahya's process and achieve higher accuracy in the updated velocity by inclusion of the reflector dip as an additional parameter.

Another MVA principle is to follow migrated reflection events through the image domain under variation of the migration velocity (Fomel, 1994; Liptow and Hubral, 1995). Hubral et al. (1996) used the term *image waves* to describe such a process of transforming time-migrated images according to the changes in migration velocity. Schleicher et al. (1997) derived equations for remigration trajectories in the zero-offset case and connected the concept to that of residual migration. In a related way, Adler (2003) described the change in the superposition of seismic data along isochrons at a predicted image point as a function of the velocity perturbation, a process he called Kirchhoff image propagation. Fomel (2003a,b) further developed and tested the velocity-continuation or image-wave concept for the prestack situation.

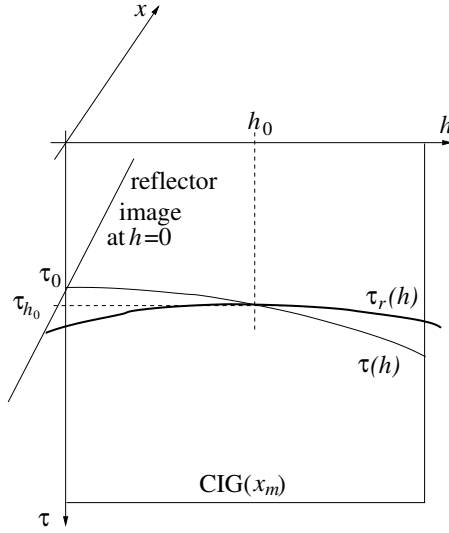


Figure 1: The residual moveout of a dipping reflector in a single CIG at x_m after migration with a wrong velocity is described by curve $\tau(h)$. However, the image of a unique reflection point moves through the whole migrated data volume along the remigration trajectory $\tau_r(h)$. The remigration trajectory can be approximated from information found at point h_0, τ_{h_0} . For details, see text.

Velocity continuation can be also used on migrated diffractions (Fomel et al., 2007; Novais et al., 2008) for MVA. Based on velocity continuation, Coimbra et al. (2011, 2012, 2013b) recently introduced a new process of extracting velocity updates from the moveout of incorrectly migrated diffraction events by tracing so-called remigration trajectories to their focus point in post-stack migrated images, and Coimbra et al. (2013a) extended their work to the prestack case. This technique makes use of local-slope information extracted from the data with the help of stacks along local trial surfaces. In this work, we modify this remigration-trajectory MVA method to make it suitable for an application to reflection events in prestack data. Tests on synthetic data from a simple model and on the Sigsbee2B data confirm the potential of our method to produce a plausible velocity model in a region with strong dip variations.

THEORETICAL DESCRIPTION

We are looking for an expression for the remigration trajectory, that is, a formula that describes the position of a reflection point in the prestack-migrated data volume as a function of migration velocity. For the mathematical derivation, we consider a horizontal reflector below a constant-velocity overburden with (true) average medium velocity v . We look at its time-migrated image for half-offset h , obtained with the (incorrect) migration velocity v_m . We start from the expression of Al-Yahya (1989) for the reflector position in a single common-image gather (Figure 1),

$$\tau(h) = \sqrt{\tau_0^2 + 4h^2 \left(\frac{1}{v^2} - \frac{1}{v_m^2} \right)}, \quad (1)$$

where τ_0 is the vertical time at zero-offset. Solving this expression for τ_0 at two half-offsets h and h_0 and equaling the results at h and h_0 yields the relationship between migrated times $\tau(h_0) = \tau_{h_0}$ at h_0 and $\tau(h) = \tau_h$ at h as

$$\tau(h) = \sqrt{\tau_{h_0}^2 + 4(h^2 - h_0^2) \left(\frac{1}{v^2} - \frac{1}{v_m^2} \right)}. \quad (2)$$

Additionally, based on the kinematics analysis of velocity continuation, Fomel (2003b) approximates

the dislocation out of the CIG up to second order in h as

$$\tau_r(h, x) = \sqrt{\tau_h^2 - \frac{4(x - x_m)^2}{v_m^2 - v^2} + 4h^2 \left(\frac{1}{v_m^2} - \frac{1}{v^2} \right)}, \quad (3)$$

where t_h is given by equation (2), and where $x - x_m$ denotes the relative midpoint coordinate. The envelope of these curves at all x , determined from setting the derivative with respect to x equal to zero, determines the lateral displacement as a function of h as

$$x_r(h) = x_m + \left(\frac{v_m^2 - v^2}{4} \right) \tau_h D_h, \quad (4)$$

where D_h denotes the event dip in the common-offset section at h , given by $D_h = \left. \frac{\partial \tau_h}{\partial x} \right|_{x_m}$. For $h = 0$, equations (3) and (4) reduce to the zero-offset equations derived by Schleicher et al. (1997).

Combining equations (3) and (4), we arrive at the residual normal-moveout (RMO) expression

$$\tau_r(h) = \sqrt{\tau_h^2 \left(1 - \frac{v_m^2 - v^2}{4} D_h^2 \right) + 4h^2 \left(\frac{1}{v_m^2} - \frac{1}{v^2} \right)}. \quad (5)$$

Expressions (4) and (5) together approximately describe the dislocation of the image of a reflection point in the migrated data volume as a function of half-offset (see again Figure 1), i.e., the so-called remigration trajectory.

With these expressions, we can thus estimate whereto in the data volume a point (h_0, τ_{h_0}) in a CIG will move when the migration velocity is changed. When applying this equation to all points in a CIG at a chosen image point, we can estimate the velocity value for which the resulting set of moved points becomes closest to a horizontal line.

To calculate the image-point positions with equations (4) and (5), we need an estimate of the image time τ_h and the event dip D_h at each point in the CIG. To estimate the values for τ_h , we adjust a curve of the form of equation (2) to the migrated event within the CIG at x_m . To avoid the necessary dip estimations in all involved common-offset sections, we use that the event dip D_h at h is related to the one at h_0 as

$$D_h = D_{h_0} \frac{\tau_{h_0}}{\tau_h}. \quad (6)$$

This relationship is obtained from the derivative of equation (2) with respect to x .

To estimate the local slope D_{h_0} in the common-offset section at h_0 , we define a surface $T = T(h, x)$ as

$$T(h, x) = \tau_h + (x - x_m) D_h = \tau_h + (x - x_m) \frac{\tau_{h_0}}{\tau_h} D_{h_0}. \quad (7)$$

This surface is tangent to traveltime surface (3), if the correct value of D_{h_0} is used. This fact can be used to estimate this parameter from the data by semblance maximization using trial surfaces.

Since the residual moveout must be minimized at the correct velocity, we can choose the derivative of $\tau_r(h)$ as the objective function. Thus, the optimization condition is

$$\min_v \left\| \frac{\partial \tau_r}{\partial h} \right\|. \quad (8)$$

Here, we propose to use the above corrections in an iterative process. In this way, we are able to flatten a reflection event by an estimation of a local slope through image-wave propagation of the CIG.

APPLICATION TO A SIMPLE SYNTHETIC TEST DATA SET

We tested the MVA technique using time-remigration trajectories as outlined above on a synthetic data set from a simple test model (Figure 2). It consists of a single trough-shaped reflector separating two homogeneous half-spaces with velocities 1.7 km/s and 1.9 km/s. Note that the reflector has a slight dip on the left side of the trough and is horizontal on the right side. Moreover, there is an edge diffractor caused

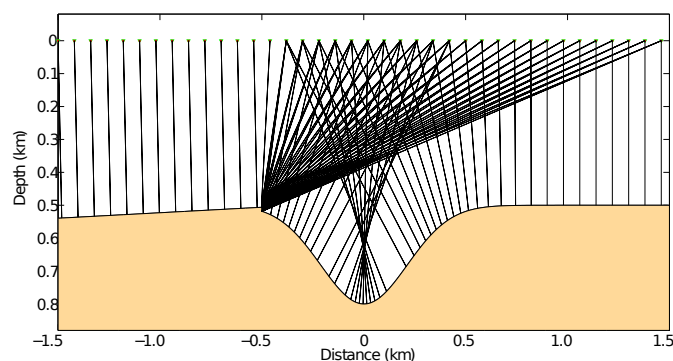


Figure 2: 2D sketch of a simple synthetic model and ray family. The model consists of two homogeneous halfspaces, separated by a reflector composed of a segment with small dip in the left portion, an edge diffractor caused by an abrupt change of direction, followed by a syncline and a horizontal reflector segment on the right side.

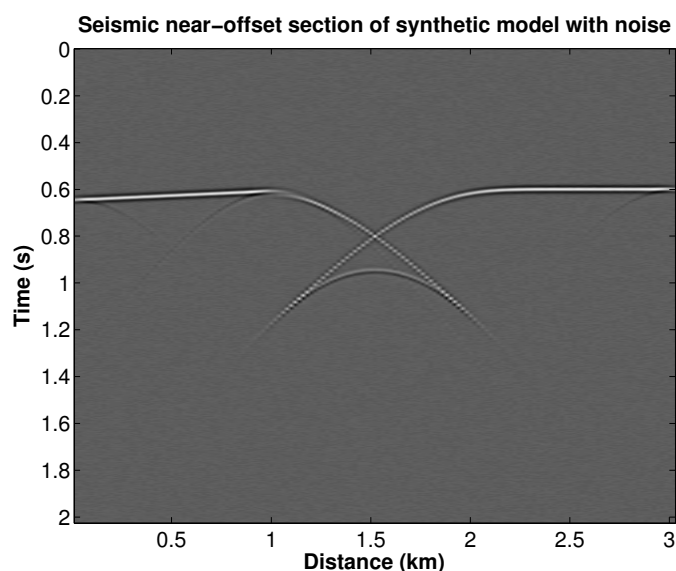


Figure 3: Noisy seismic near-offset section of the synthetic model presented in Figure 2. It was generated by Kirchhoff modeling with 151 traces at every 20 meters and a sampling rate of 4 ms and contaminated with white random noise at a level of 10% of the maximum amplitude.

by an abrupt change of direction on the left shoulder of the syncline, indicated by the set of diffraction rays plotted in Figure 2.

We used Kirchhoff modeling to generate synthetic 151 data traces (Figure 3) at every 20 meters with a sampling rate of 4 ms and contaminated those data with white random noise at a level of 10% of the maximum amplitude. The trough-shaped reflector causes a caustic, evidenced by the distorted bow-tie structure in the data (Figure 3). The diffraction event has much smaller amplitude than the reflection event.

Supposing the true velocity of the upper layer to be unknown, we time-migrated these data with a constant initial velocity (Figure 4). In this example, we chose the water velocity $v_0 = 1.5$ km/s (for land-data, one might use some known near-surface velocity). The range of possible values of the initial velocity is fairly large and not vital to the method. We immediately recognize in this migrated image that the migration velocity was not correct, because the bow-tie structure from the synclinal reflector is not completely resolved. Also note that the edge diffractor is incorrectly imaged, with a spatial separation between the two reflector segments.

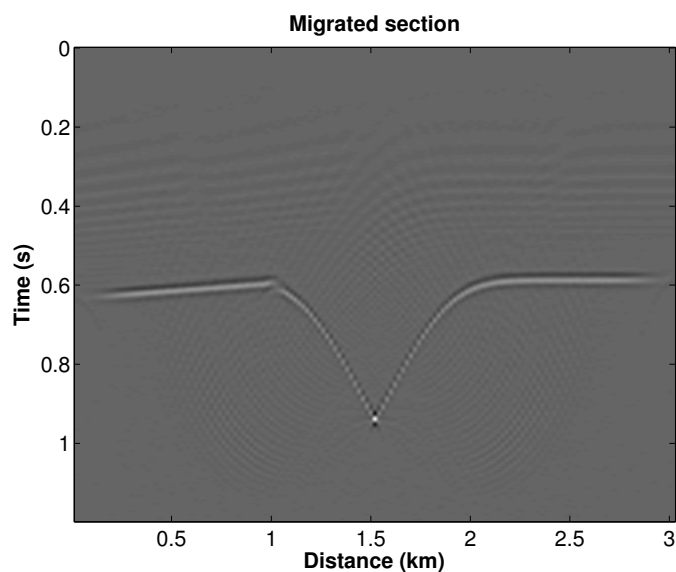


Figure 4: Time-migrated image of the seismic near-offset section of Figure 3 using a constant velocity $v_0 = 1.5$ km/s (water velocity) and a migration aperture of 101 traces.

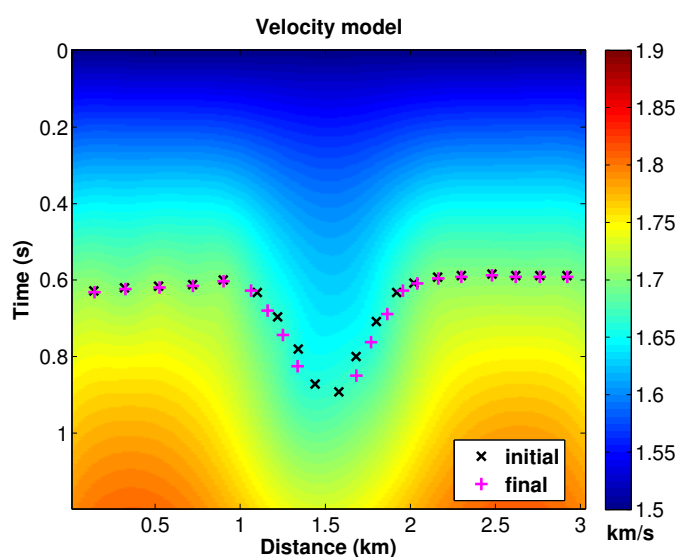


Figure 5: Updated velocity model using image point correction from constant velocity migration (one iteration). The 20 black crosses represent the initial picked points in the migrated image (Figure 6), and the pink pluses indicate the corrected coordinates for the new velocity. This model was obtained by B-spline interpolation.

In this migrated section, we select specific points on the images of reflection events (by manual clicks). The coordinates of each of these points define the present values of τ_{h_0} and x_m . In the CIG at x_m , we automatically determine the event slope D_{h_0} at h_0 as indicated in the context of equation (7). This slope value allows to apply an improved moveout correction to the chosen CIG according to equation (5). Moveout minimization according to equation (8) yields an improved velocity value and a corrected position for the chosen point in the image.

Figure 5 shows velocity model obtained after a single iteration of the describe MVA procedure. The black crosses represent the 20 points initially picked in the migrated image of Figure 4, and the pink pluses indicate their corrected coordinates in the improved velocity model. This model was obtained by B-spline

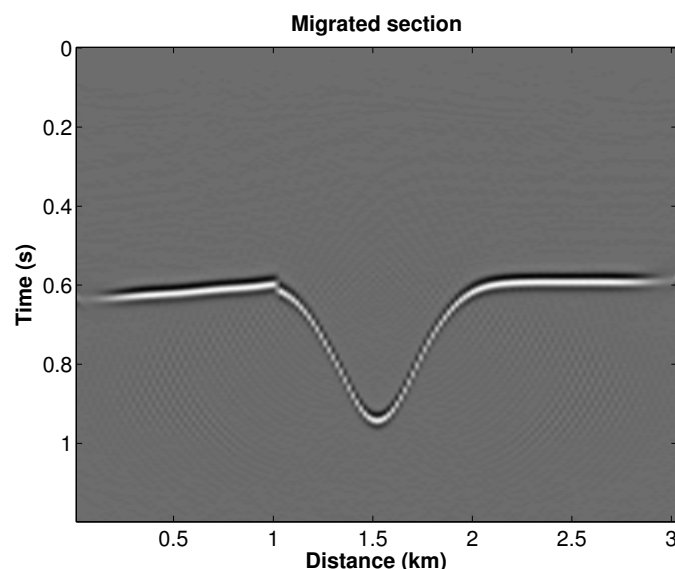


Figure 6: Final migrated image stack after velocity extraction using one iteration of image point correction. The migration aperture used was 101 traces.

interpolation of the information at the picked points. Note that the determined velocity in the region of the picks is closely approximating the true velocity of 1.7 km/s, with a maximum error of about 2%. Values outside the region of the picks are artifacts of the interpolation and carry no meaning.

Figure 6 depicts the stack of all migrated images obtained from migrating all common-offset sections with the model of Figure 5. We see that MVA by time-remigration trajectories nicely positioned all parts of the reflector very closely to their true positions, confirming the good velocities in the reflector region.

APPLICATION TO THE SIGSBEE2B DATA

For a more realistic test, we applied the described MVA technique to a subset of the Sigsbee2B NFS (no free surface) data set, so as to analyze complex structures like syncline segments over a salt structure. The Sigsbee2B data contains traces at every 45.7 meters with a sampling rate of 8 ms. Figures 7 and 8 show the Sigsbee2B stratigraphic velocity model and a short-offset section, respectively.

Reference images

In order to simulate a plausible velocity model and its respectively migrated image, we computed the interval (v_{int}) and the root-mean-square (v_{rms}) velocity models in pseudo-time from the stratigraphic velocity, both using vertical conversion only. The pseudo-time interval velocity model (Figure 9) gives us an approximate idea of where to look for reflector images in the migrated image. The average velocity v_{rms} (Figure 10) indicates acceptable migration velocity values, though probably laterally mispositioned.

Therefore, rather than using this model for comparisons to those obtained with our method, we use v_{rms} to migrate the Sigsbee2B data set. Figure 11 shows the time-migrated image of the seismic near-offset section using the average velocity v_{rms} and migration aperture equal to 241 traces.

By correlating the time-migrated image of Figure 11 with the pseudo-time interval velocity model of Figure 9, we can easily identify the positions of most reflectors. We note that the shallow events and most sedimentary parts are well focused, including the shallow diffraction events. However, the salt bottom and deepest parts are out of focus, indicating that the model of Figure 10 is only acceptable down to a certain depth. We will use the image of Figure 11 as a reference for comparison with the images obtained with the models from our method.

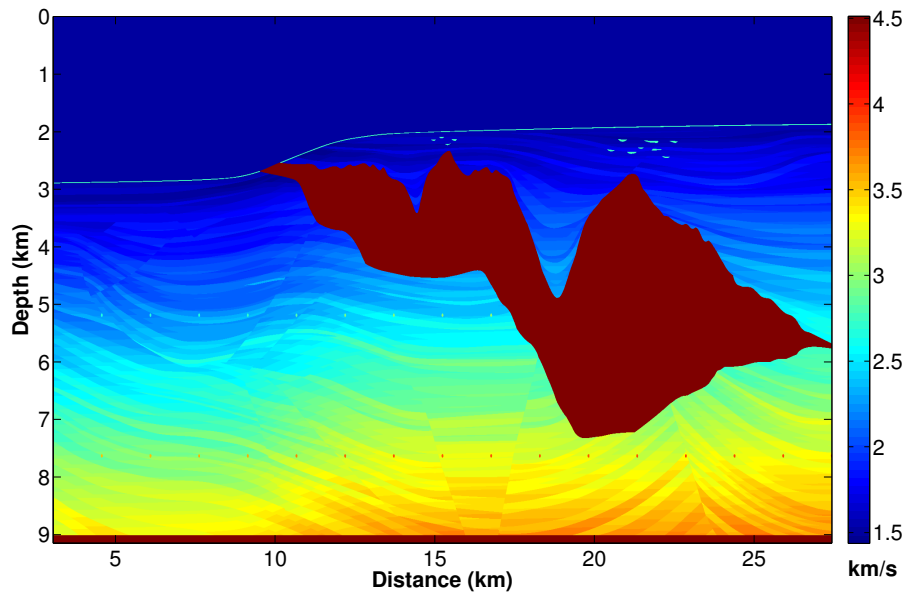


Figure 7: Complete Sigsbee2B stratigraphic velocity model.

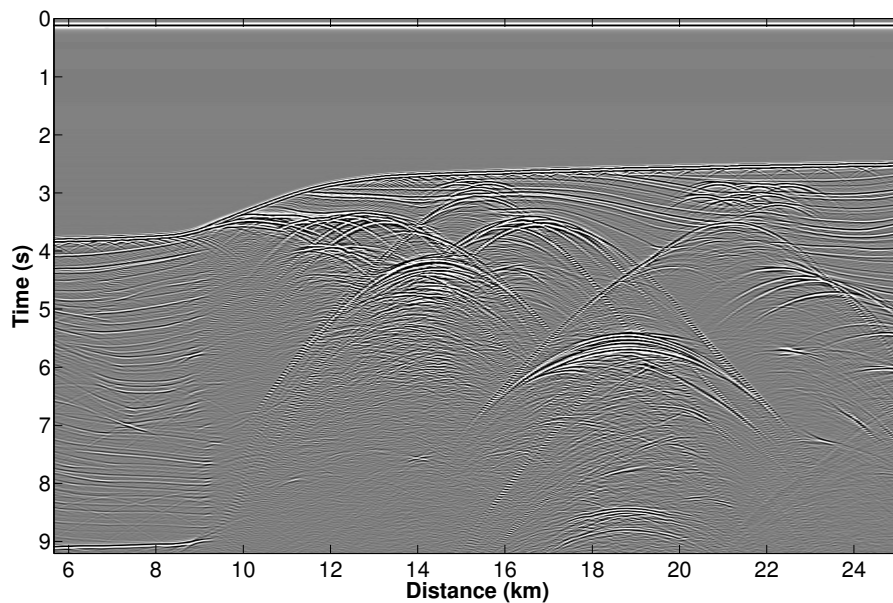


Figure 8: Seismic near-offset section of the complete Sigsbee2B data.

Velocity analysis

Since the Sigsbee2B data simulate a marine data set, we know the velocity of the first layer to be constant water velocity $v_0 = 1.5$ km/s. Thus, we choose this velocity for the first migration. Figure 12 depicts the migrated image obtained from the short-offset data of Figure 8. The migration aperture used was 141 traces. As expected, this first migration is not able to resolve the bow-tie structure or focus the reflection energy.

Next, in order to apply the MVA by time-remigration trajectory as discussed above, we picked 254 points on some of the most prominent migrated events in the image of Figure 12. At the positions of these picks, we extract local slopes in the common-offset section and then minimize the residual moveouts in the respective CIGs. Figure 13 shows the locations of our picks (black crosses) and their corrected positions (pink pluses) overlain on the resulting updated velocity model. As before, we used

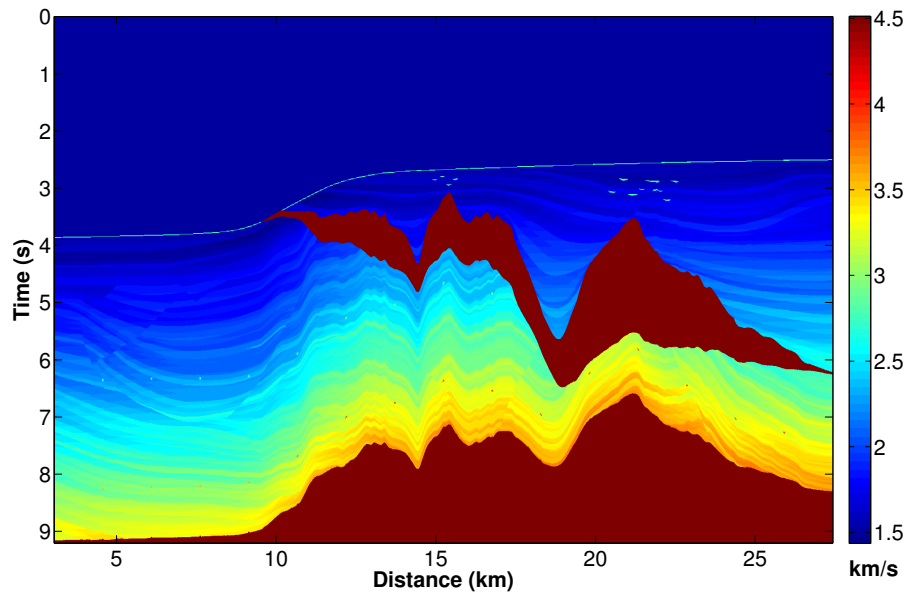


Figure 9: Sigsbee2B vertical pseudo-time interval velocity model (v_{int}).

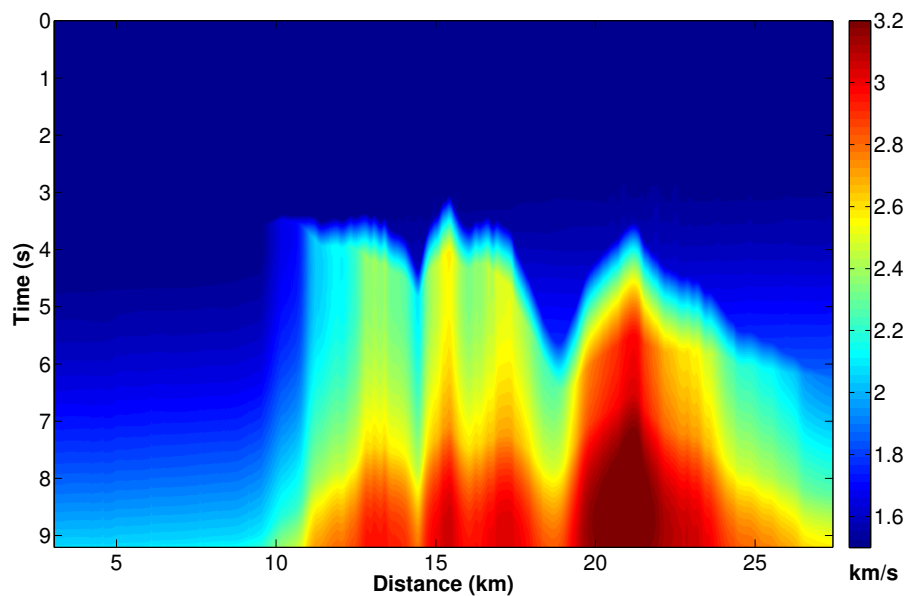


Figure 10: Sigsbee2B vertical pseudo-time root-mean-square velocity model (v_{rms}).

B-splines to interpolate the velocity model in the complete region. It is easy to see that the picked image points are moved further away from their original positions in the (large) syncline region between 16 and 22 km, where the difference between the initial and true velocities is larger than in the upper part of the model, where the water velocity is rather close to the true medium velocity.

We then used the velocity model of Figure 13 for a second migration. The result is depicted in Figure 14. We immediately recognize that the shallower parts of the salt top have been nicely improved in this image, indicating that the velocity model in this region already has reached acceptable quality. Certainly, the same cannot be said of the salt flanks. Therefore, we have repeated the procedure of reflector picking and velocity updating for a second set of points picked in this new migrated image.

Figure 15 shows the velocity model after this second iteration together with the 322 picked points (black crosses) and their updated positions (pink pluses). We note that the displacements are smaller than

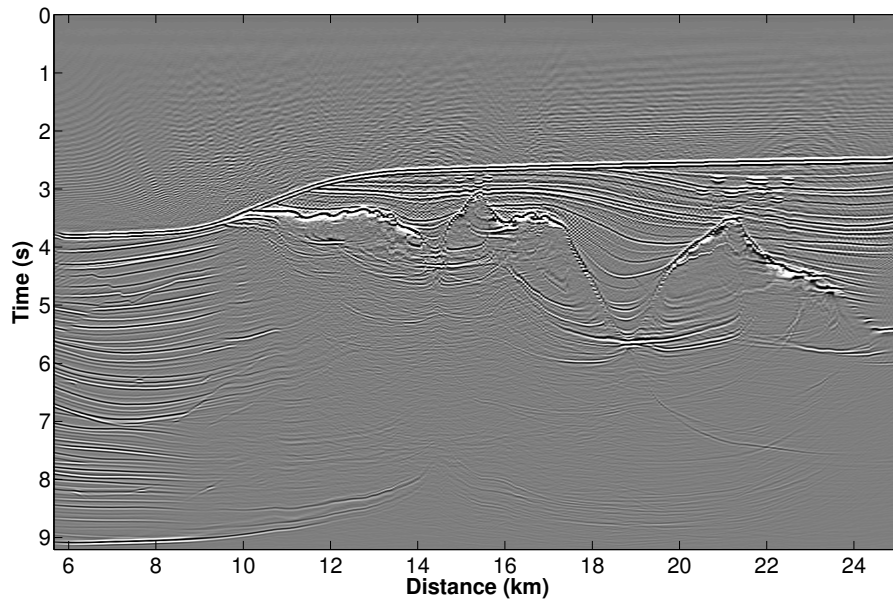


Figure 11: Time-migrated image of the seismic near-offset section using the average velocity v_{rms} (Figure 10) and migration aperture equal to 241 traces.

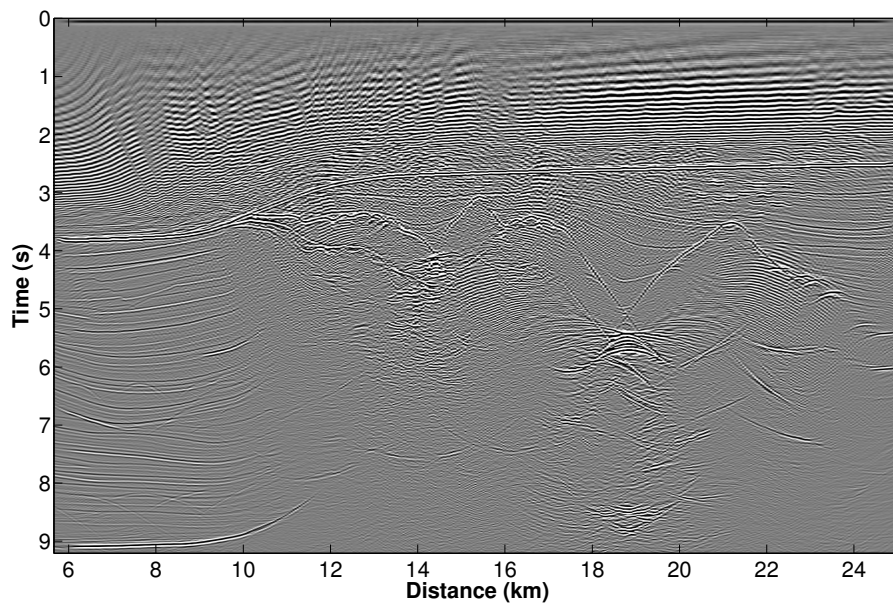


Figure 12: Time-migrated image of the seismic near-offset section using a constant velocity $v_0 = 1.5$ km/s (water velocity) and migration aperture equal to 141 traces.

in Figure 13, indicating convergence of the method. Note that the deeper events in the central part of the model are still not focused in the image and could therefore not be picked. The velocity model in this region is thus just obtained from B-splines extrapolation and must be taken with care. Further iterations would be necessary to improve the image in this region.

The migrated image corresponding to this velocity model is depicted in Figure 16. For this migration, we used a migration aperture of 241 traces. In comparison to Figure 14, the flanks of the (large) synclinal structure are much better focused and the bottom of the trough is correctly positioned. Furthermore, we have also obtained an improvement in the left portion of the salt base. Actually, the image of Figure 16

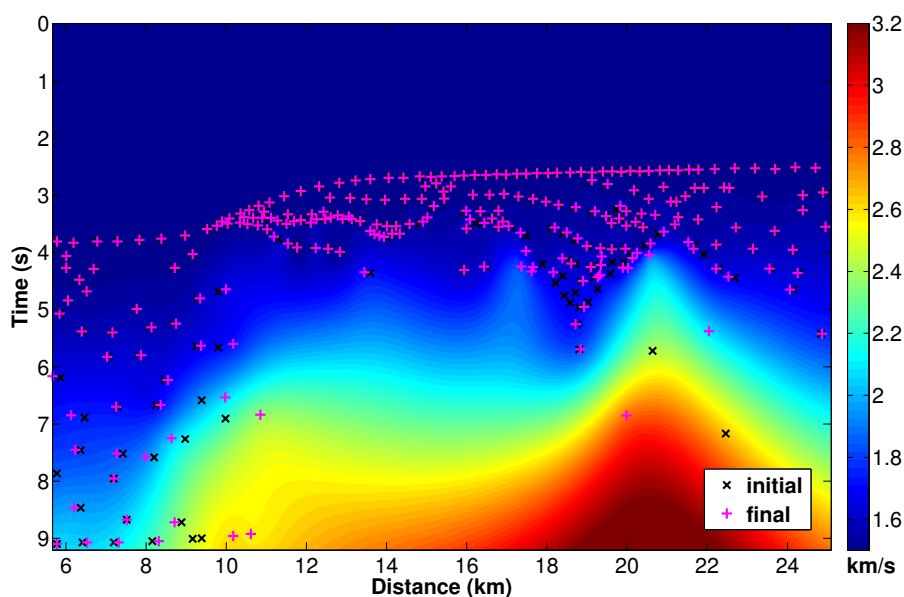


Figure 13: Velocity model extracted using image-point correction with remigration trajectories after constant-velocity migration (first iteration). The 254 black crosses represent the initial picked points in the migrated image of Figure 12, and the pink pluses indicate their corrected coordinates for the updated velocity. The overall model was obtained by B-spline interpolation.

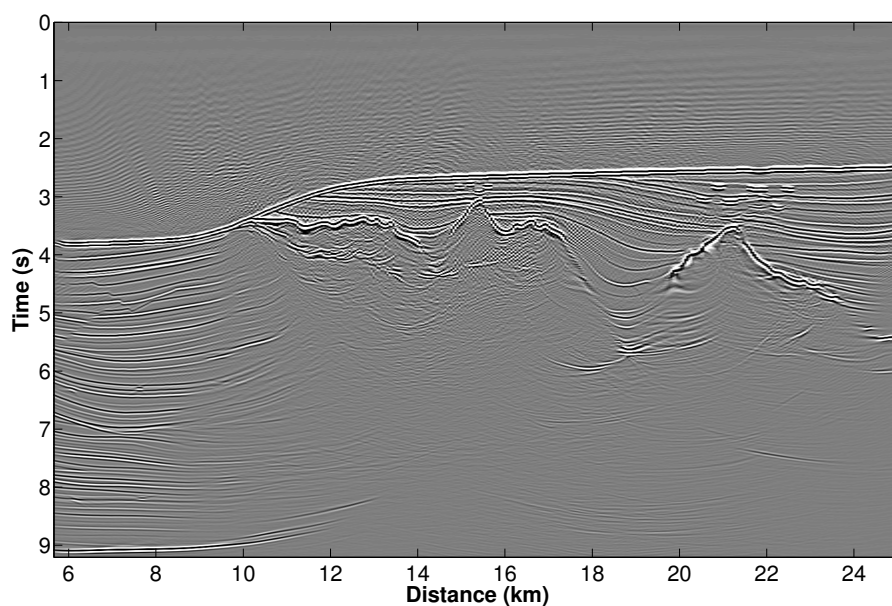


Figure 14: Migrated image after velocity extraction using one iteration of image point correction. The migration aperture used was 141 traces.

is already visibly better than the one of Figure 11, indicating that the model of Figure 15 is already better than the vertically converted model of Figure 10.

To evaluate the quality of the final velocity model in more detail, let us look at six selected CIGs (Figure 17). On the whole, it is easy to observe that the strongest events, mainly the shallow ones, were completely flattened. The first CIG at 7.65 km (Figure 17(a)) lies in the most simple region where there are no abrupt velocity variation. In Figure 17(a), all major events were flattened, including the diffraction

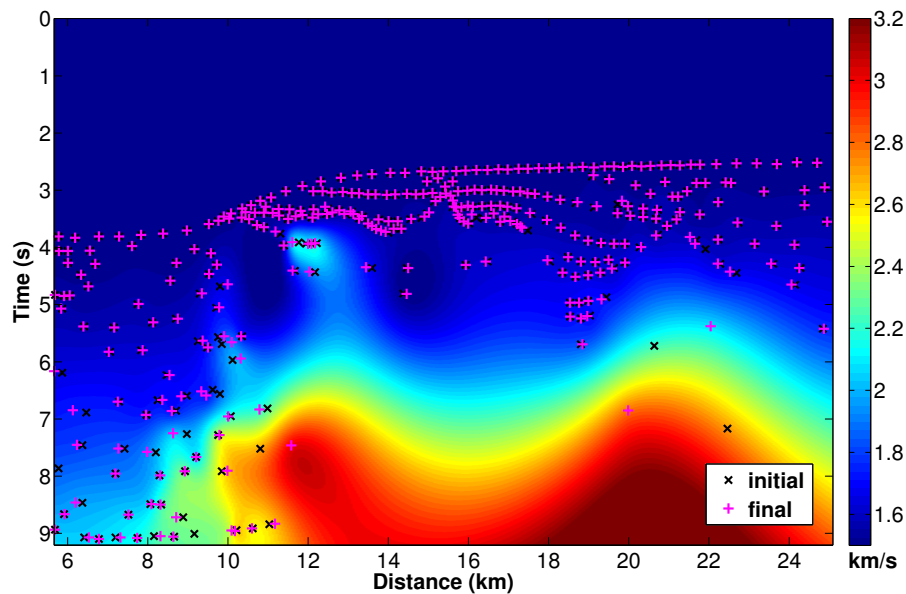


Figure 15: Velocity model after second iteration. The 322 black crosses represent the picked points in the migrated image of Figure 14, and the pink plusses indicate their corrected coordinates.

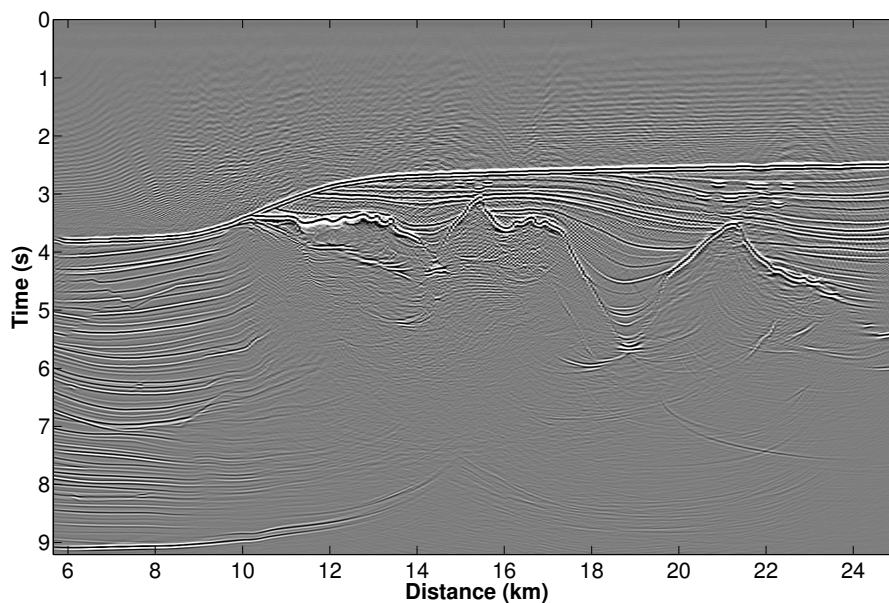


Figure 16: Final migrated image stack after two iterations of velocity extraction using remigration trajectories. The migration aperture was 241 traces.

event below 6 seconds, and the deepest flat salt layer at about 9 seconds (see also Figure 16). In the CIG at 13.68 km (Figure 17(b)), we can observe that the salt top (~ 3.6 s) and the diffraction event (~ 5.2 s) were well flattened, but the salt bottom (~ 4.2 seconds) still needs improvement at larger offsets. The third CIG at 16.56 km (Figure 17(c)) allow to analyze the edge diffraction at the salt bottom at about 4.2 seconds (see also the model in Figure 7). It shows that our method flattened the diffraction event. The fourth CIG at 18.85 km (Figure 17(d)) represents the central part of the Sigsbee2B syncline. Here, we call attention to the high amplitudes below 5 seconds due to multiple reflections in this syncline. Nevertheless, it is possible to observe the nearly flattened event of the bottom of the trough at about 5.6 seconds. The fifth

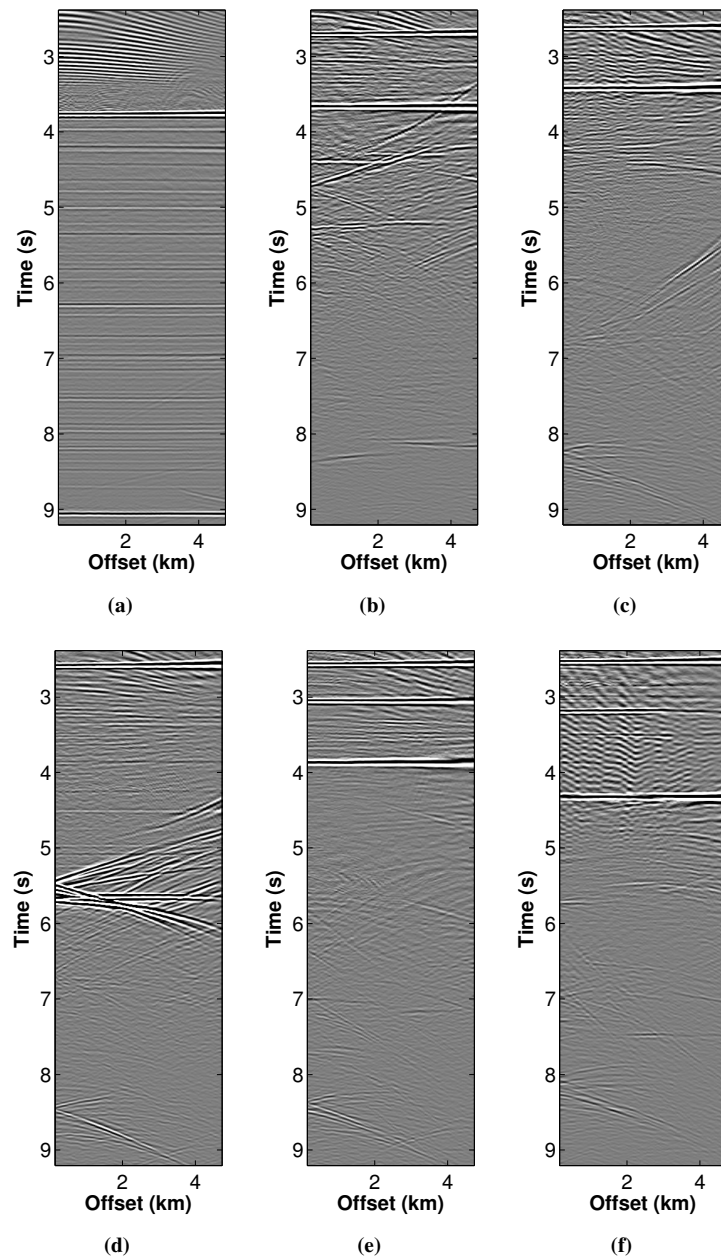


Figure 17: Common-image gathers at (a) 7.65 km, (b) 13.68 km, (c) 16.56 km, (d) 18.84 km, (e) 20.54 km, and (f) 22.32 km.

CIG at 20.54 km (Figure 17(e)) shows the right portion of the syncline, where the salt structure is thicker and where shallow diffractors are present. We note that down to the salt top, all events are nicely flattened. The last CIG at 22.32 km (Figure 17(f)) enables us to evaluate the right portion of the salt structure, with a thinning of the salt body and a greater dip variation of its top. As expected, the deeper events below the salt are not well imaged with the present velocity model.

The coherence panel associated with the migrated image provides another indication of where the obtained velocity model can already be trusted and where further improvement is required. Figure 18 shows the horizontal semblance in the corresponding CIG at each point of the migrated image of Figure 16. All main events down to the salt top are well imaged, and even the edge diffractor at the salt bottom is clearly visible. The slight residual moveout of the bottom-of-the-trough reflection in the CIG of Figure 16 results

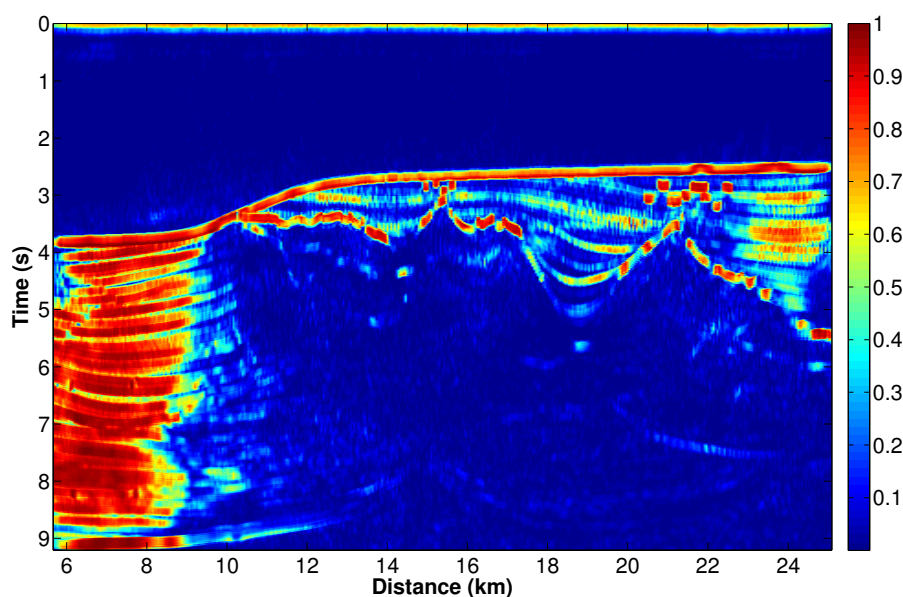


Figure 18: Coherence panel after the second iteration.

in its poor visibility in this panel.

From the analysis of the coherence panel, the CIGs and the final migrated image, we conclude that MVA using time-remigration trajectories constitutes a powerful tool to improve the positioning of key reflectors in a migrated image and update the velocity model correspondingly, at least in sedimentary regions. The focused edge diffraction event at the salt bottom gives rise to hopes that the method will also work in more complex areas. The computational cost of the technique is determined by the cost of prestack time migration in each iteration. Intermediate computations are negligible. Further investigations will have to show whether the picking of selected reflection event points can be carried out in an automated way.

When testing our method, we noted that the resulting velocity models were strongly dependent on the method chosen to interpolate the velocity between the positions of the picks. However, the resulting images were rather similar to each other, providing another confirmation for the robustness of time migration with respect to velocity errors. For the presentation in this work, we chose the models obtained by B-splines interpolation of Matlab (Sandwell, 1987).

CONCLUSIONS

We have developed a tool that uses the estimation of local kinematic attributes of selected events in seismic data to update the velocity model and improve the positioning of key reflectors. The method is based on image-wave propagation in the common-image-gather (CIG) domain described by the means of time-remigration trajectories in the prestack time-migrated domain. Such a trajectory is defined as the set of points where a certain point on a reflection event is migrated to as a function of migration velocity.

The methods consists of analyzing the local slope of selected key reflections and determining the velocity value for which an approximate residual-moveout expression is minimized. The advantage of this procedure over conventional MVA methods is that the RMO expression follows the events outside a fixed CIG. In our numerical tests, this led to acceptable velocity models in very few iterations, even if the starting model was simply constant water velocity. The sedimentary shallow part of the Sigsbee2B model was satisfactorily resolved in two iterations. The computational cost of the technique is determined by the cost of prestack time migration in each iteration. Intermediate computations are negligible.

ACKNOWLEDGEMENTS

This research was supported by Petrobras and CGG as well as the Brazilian research agencies CNPq, FAPESP, FINEP, and CAPES. The second author (HBS) thanks CGG-Brazil for his fellowship. Additional

support for the authors was provided by the sponsors of the *Wave Inversion Technology (WIT) Consortium*. We would like to thank the SMAART JV for providing the Sigsbee2B NFS dataset.

REFERENCES

- Adler, F. (2003). Kirchhoff image propagation. *Geophysics*, 67(1):126–134.
- Al-Yahya, K. M. (1989). Velocity analysis by iterative profile migration. *Geophysics*, 54(06):718–729.
- Coimbra, T. A., de Figueiredo, J. J. S., Novais, A., and Schleicher, J. (2011). Migration velocity analysis with diffraction events using residual moveout. *Annual WIT report*, 15:57–70.
- Coimbra, T. A., de Figueiredo, J. J. S., Novais, A., Schleicher, J., and Arashiro, S. (2013a). Migration velocity analysis using residual diffraction moveout in the pre-stack depth domain. *Annual WIT report*, 17. This report.
- Coimbra, T. A., de Figueiredo, J. J. S., Schleicher, J., Novais, A., and Costa, J. (2013b). Migration velocity analysis using residual diffraction moveout in the poststack depth domain. *Geophysics*, 78(3):S125–S135.
- Coimbra, T. A., de Figueiredo, J. J. S., Schleicher, J., Novais, A., and Costa, J. C. (2012). Migration velocity analysis with diffraction events using residual moveout: Application to SIGSBEE 2B data. *Annual WIT report*, 16:45–58.
- Fomel, S. (1994). Method of velocity continuation in the problem of seismic time migration. *Russian Geology and Geophysics*, 35(5):100–111.
- Fomel, S. (2003a). Time migration velocity analysis by velocity continuation. *Geophysics*, 68(5):1662–1672.
- Fomel, S. (2003b). Velocity continuation and the anatomy of residual prestack time migration. *Geophysics*, 67(5):1650–1661.
- Fomel, S., Landa, E., and Taner, M. T. (2007). Poststack velocity analysis by separation and imaging of seismic diffractions. *Geophysics*, 72(6):U89–U94.
- Hubral, P., Tygel, M., and Schleicher, J. (1996). Seismic image waves. *Geophysical Journal International*, 125:431–442.
- Liptow, F. and Hubral, P. (1995). Migrating around in circles. *The Leading Edge*, 14(11):1125–1127.
- Liu, Z. and Bleistein, N. (1995). Migration velocity analysis: Theory and an iterative algorithm. *Geophysics*, 60(01):142–153.
- Novais, A., Costa, J., and Schleicher, J. (2008). GPR velocity determination by image-wave remigration. *Journal of Applied Geophysics*, 65(2):65–72.
- Sandwell, D. T. (1987). Biharmonic spline interpolation of GEOS-3 and SEASAT altimeter data. *Geophysical Research Letters*, 2:139–142.
- Sattlegger, J. W. (1975). Migration velocity determination: Part I. philosophy. *Geophysics*, 40(1):1–5.
- Schleicher, J. and Biloti, R. (2007). Dip correction for coherence-based time migration velocity analysis. *Geophysics*, 72(1):S431–S48.
- Schleicher, J., Hubral, P., and Höcht, G. (1997). Seismic constant-velocity remigration. *Geophysics*, 62(2):589–597.
- Zhu, J., Lines, L., and Gray, S. (1998). Smiles and frowns in migration/velocity analysis. *Geophysics*, 63(04):1200–1209.